The Astrophysical Journal Letters, 770:L39 (6pp), 2013 June 20 doi:10.1088/2041-8205/770/2/L39
© 2013. The American Astronomical Society. All rights reserved. Printed in the U.S.A.

QUIESCENT GALAXIES IN THE 3D-HST SURVEY: SPECTROSCOPIC CONFIRMATION OF A LARGE NUMBER OF GALAXIES WITH RELATIVELY OLD STELLAR POPULATIONS AT $z \sim 2$

Katherine E. Whitaker[1,8], Pieter G. van Dokkum[2], Gabriel Brammer[3], Ivelina G. Momcheva[2], Rosalind Skelton[2], Marijn Franx[4], Mariska Kriek[5], Ivo Labbé[4], Mattia Fumagalli[4], Britt F. Lundgren[6], Erica J. Nelson[2], Shannon G. Patel[4], and Hans-Walter Rix[7]

[1] Astrophysics Science Division, Goddard Space Flight Center, Code 665, Greenbelt, MD 20771, USA; kate.whitaker@nasa.gov
[2] Department of Astronomy, Yale University, New Haven, CT 06520, USA
[3] European Southern Observatory, Alonso de Córdova 3107, Casilla 19001, Vitacura, Santiago, Chile
[4] Sterrewacht Leiden, Leiden University, NL-2300 RA Leiden, The Netherlands
[5] Department of Astronomy, University of California, Berkeley, CA 94720, USA
[6] Department of Astronomy, University of Wisconsin, Madison, WI 53706, USA
[7] Max Planck Institut fur Astronomie, Königstuhl 17, D-69117 Heidelberg, Germany
Received 2013 March 21; accepted 2013 May 9; published 2013 June 10

ABSTRACT

Quiescent galaxies at $z \sim 2$ have been identified in large numbers based on rest-frame colors, but only a small number of these galaxies have been spectroscopically confirmed to show that their rest-frame optical spectra show either strong Balmer or metal absorption lines. Here, we median stack the rest-frame optical spectra for 171 photometrically quiescent galaxies at $1.4 < z < 2.2$ from the 3D-HST grism survey. In addition to Hβ (λ4861 Å), we unambiguously identify metal absorption lines in the stacked spectrum, including the G band (λ4304 Å), Mg I (λ5175 Å), and Na I (λ5894 Å). This finding demonstrates that galaxies with relatively old stellar populations already existed when the universe was ~3 Gyr old, and that rest-frame color selection techniques can efficiently select them. We find an average age of $1.3^{+0.1}_{-0.3}$ Gyr when fitting a simple stellar population to the entire stack. We confirm our previous result from medium-band photometry that the stellar age varies with the colors of quiescent galaxies: the reddest 80% of galaxies are dominated by metal lines and have a relatively old mean age of $1.6^{+0.5}_{-0.4}$ Gyr, whereas the bluest (and brightest) galaxies have strong Balmer lines and a spectroscopic age of $0.9^{+0.2}_{-0.1}$ Gyr. Although the spectrum is dominated by an evolved stellar population, we also find [O III] and Hβ emission. Interestingly, this emission is more centrally concentrated than the continuum with $L_{\rm O\,III} = 1.7 \pm 0.3 \times 10^{40}$ erg s^{-1}, indicating residual central star formation or nuclear activity.

Key words: galaxies: evolution – galaxies: formation – galaxies: high-redshift

Online-only material: color figures

1. INTRODUCTION

In the nearby universe, the most massive galaxies almost always have little ongoing star-formation and red colors that exhibit a remarkably small intrinsic scatter (e.g., Bower et al. 1992). These red, quiescent galaxies form a well-defined color–mass relation known as the "red sequence." Photometric studies of large, representative samples of galaxies based on broadband and medium-band photometry have pushed the detection of the red sequence out to $z \sim 2$ (e.g., Williams et al. 2009; Whitaker et al. 2011; Brammer et al. 2011; Nicol et al. 2011). However, only a small fraction of these distant quiescent galaxies have been spectroscopically confirmed (e.g., Cimatti et al. 2004, 2008; Daddi et al. 2005; Kriek et al. 2006, 2008, 2009; van Dokkum & Brammer 2010; van de Sande et al. 2011, 2012; Onodera et al. 2012; Toft et al. 2012; Bezanson et al. 2013).

Interestingly, most distant quiescent galaxies with high-quality rest-frame optical spectra appear to exhibit young ages, showing strong Balmer absorption lines (e.g., van de Sande et al. 2012; Bezanson et al. 2013). This could imply that the bulk of high-redshift quiescent galaxies were recently quenched. However, most spectroscopic studies in the literature are biased toward the brightest (and consequently youngest) of such galaxies. Therefore, spectroscopic ages for a representative sample of quiescent galaxies remains elusive.

Owing to the near-infrared (NIR) slitless spectroscopic capabilities provided by the Wide-Field Camera 3 (WFC3) on the *Hubble Space Telescope* (*HST*), it is now possible to obtain low-resolution spectroscopy of a mass-limited sample of quiescent galaxies at $z \sim 2$. In this Letter, we stack the spectra of 171 quiescent galaxies at $z \sim 2$ and demonstrate that they have absorption features indicative of evolved stellar populations. Furthermore, with ages derived from the stacked grism spectra, we are in a unique position to test what drives the color spread of quiescent galaxies for the first time.

We assume a ΛCDM cosmology with $\Omega_M = 0.3$, $\Omega_\Lambda = 0.7$, and $H_0 = 70$ km s^{-1} Mpc^{-1} throughout the Letter. All magnitudes are given in the AB system.

2. DATA

The 3D-HST treasury program (Brammer et al. 2012a), a 248 orbit NIR spectroscopic survey with the *HST*/WFC3 G141 grism, provides spatially resolved low-resolution spectra of all objects in 5 well-studied extragalactic fields to a 5σ depth for continuum magnitudes of $H_{\rm F140W} \sim 23$. 3D-HST has targeted the AEGIS, COSMOS, GOODS-S, and Ultra Deep Survey (UDS) fields, as well as incorporated publicly available data in the GOODS-N field (GO:11600; PI:Weiner). WFC3 imaging for all five fields is available from the CANDELS survey (Grogin et al. 2011; Koekemoer et al. 2011). With a wavelength range of $1.10\ \mu{\rm m} < \lambda < 1.65\ \mu$m, the prominent age-dependent H$\beta\lambda$4861 and Mgλ5175 absorption features in quiescent

[8] NASA Postdoctoral Program Fellow.

galaxies at $z \sim 2$ are observable. The first-order dispersion of the G141 grism is 46 Å pixel^{-1} ($R \sim 130$) with a spatial resolution of 0.″12, sampled with 0.″06 pixels; as the spectra have high spatial resolution and low spectral resolution, the line width almost exclusively reflects the size of the galaxy in the dispersion direction.

The sample used in this Letter is selected from WFC3-selected photometric catalogs generated from the *HST* Advanced Camera for Surveys and WFC3 images of the CANDELS and 3D-HST survey fields, along with ancillary ground-based optical and NIR images and mid-IR images with *Spitzer*/IRAC using a methodology similar to that described by Whitaker et al. (2011). A full description of these catalogs is beyond the scope of this Letter and will be described in a forthcoming paper (R. Skelton et al., in preparation). We extract a two-dimensional flux-calibrated WFC3/G141 grism spectrum for every object in the photometric catalog with $H_{\rm F140W} < 24$. Details of the reduction and extraction of the grism spectra, including accounting for the contamination of overlapping objects, are provided by Brammer et al. (2012a, 2012b).

To determine the galaxy redshifts, we first compute a purely photometric redshift from the photometry, using the EAZY code (Brammer et al. 2008). We then fit the full two-dimensional grism spectrum separately with a combination of the continuum template taken from the EAZY fit and a single emission-line-only template with fixed line ratios taken from the Sloan Digital Sky Survey (SDSS) composite star-forming galaxy spectrum of Dobos et al. (2012). The final grism redshift, `z_grism`, is determined on a finely sampled redshift grid with the photometry-only redshift probability distribution function used as a prior. This method is somewhat more flexible than that originally described by Brammer et al. (2012a), but the redshift precision is similar with $\sigma \sim 0.0035(1+z)$. Finally, rest-frame colors and stellar population parameters are computed from the photometry with the EAZY and FAST (Kriek et al. 2009) codes, respectively, with the redshift fixed to `z_grism` and assuming a Chabrier (2003) initial mass function.

3. SAMPLE SELECTION

A standard method for discriminating high-redshift quiescent galaxies from star-forming galaxies is selecting on the rest-frame $U-V$ and $V-J$ colors (e.g., Labbé et al. 2005; Wuyts et al. 2007; Williams et al. 2009; Bundy et al. 2010; Cardamone et al. 2010; Whitaker et al. 2011; Brammer et al. 2011; Patel et al. 2012); quiescent galaxies have strong Balmer/4000 Å breaks, characterized by red $U-V$ colors and relatively blue $V-J$ colors.

Following the definition of Whitaker et al. (2012), our quiescent selection box is shown in Figure 1, with the larger 3D-HST parent sample at $1.4 < z < 2.2$ shown in gray scale. Using the dotted line in Figure 1 ($(U-V) = -1.25 \times (V-J) + 2.85$), we further divide our quiescent sample into "younger" (blue) and "older" (red) galaxies (Section 5). The nature of the stellar populations of galaxies with rest-frame colors close to the quiescent/star-forming division is not clear and we therefore restrict our analysis to be more conservative by 0.08 mag (excluding those galaxies with high transparency in Figure 1). We select galaxies at $1.4 < z_{\rm grism} < 2.2$ with stellar masses $\log(M_\star) > 10.5\ M_\odot$, further restricting our sample to require >75% wavelength coverage of the grism spectrum with <50% of the pixels flagged as bad. The grism spectra of quiescent galaxies do not have strong emission line features and therefore the redshifts may not be reliable beyond certain magnitude limits; we additionally require that we detect the continuum at $\gtrsim 5\sigma$ per resolution element in the one-dimensional spectrum ($H_{\rm F140W} < 22.8$), removing the faintest 20% of galaxies.

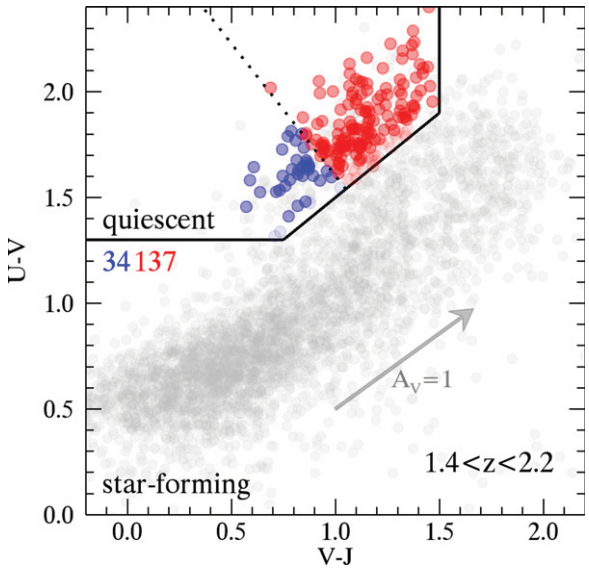

Figure 1. Rest-frame $U-V$ and $V-J$ color selection of quiescent galaxies, further separating the sample into two bins of younger (blue) and older (red) quiescent galaxies in Section 5. All galaxies with $H_{\rm F140W} < 24$ are shown in gray scale.

(A color version of this figure is available in the online journal.)

4. QUIESCENT STACKS

Although the individual galaxies are too faint to discern spectral features, by stacking the spectra of our final sample of 171 galaxies, we can achieve the necessary signal-to-noise ratio to robustly identify absorption features in a large well-defined high-redshift sample for the first time. To normalize the spectra, we shift to the rest-frame and interpolate the flux values to a new wavelength grid with 10 Å width bins. Next, we fit the continuum in each spectrum with a third-order polynomial, masking regions around prominent absorption features. After dividing by the continuum, we determine the median flux value at each wavelength bin and smooth with a boxcar of 20 Å. The gray scale error bars are derived from 100 bootstrap iterations of the stacking analysis.

We show the stacked spectrum in Figure 2. In the top panel, we see many clear absorption features: G band (λ4304 Å) blended with Hγ(λ4341 Å), Mg I (λ5175 Å), Fe I (λ5269 Å), and Na I (λ5894 Å). These metal lines are indicative of an evolved stellar population. We caution that systematic residuals in the blue part of the spectrum are of similar strength as the emission lines. The residuals do not seem to be caused by photon noise, and show up in all stacked spectra. We have not identified the cause of these residuals. We cannot exclude errors in the stellar population synthesis models, although that is unlikely in this well-studied wavelength range.

We perform a least-squares minimization using the Vazdekis et al. (2010) models to find the best-fit age of the stack. The Vazdekis et al. (2010) models provide moderately high resolution spectral energy distributions computed assuming an instantaneous burst, solar metallicity, and a Kroupa (2001) universal initial mass function, based on the MILES (Sánchez-Blázquez et al. 2006) stellar library. We simulate the expected morphological broadening by convolving the

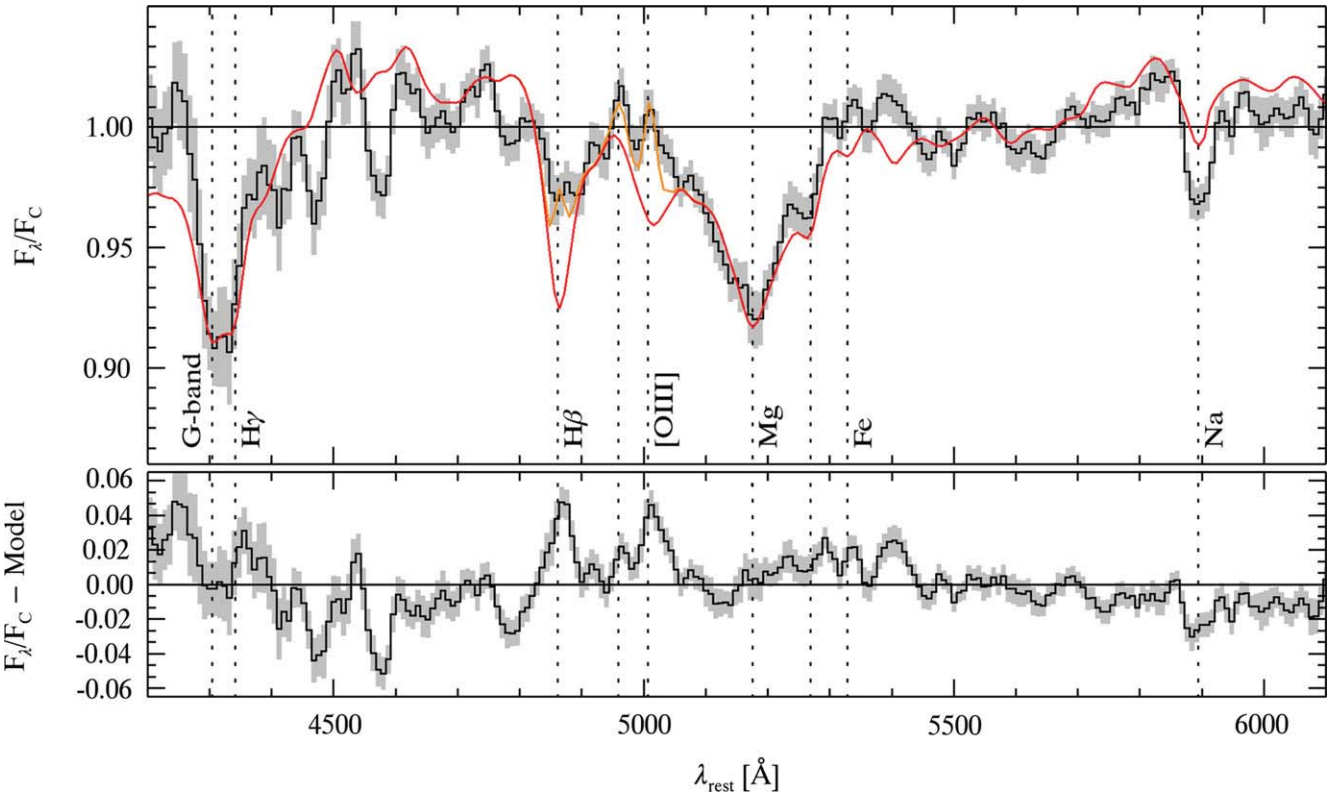

Figure 2. Median rest-frame stack of 171 quiescent galaxies (top) and the residuals after subtracting the best-fit model (red) with an age of 1.25 Gyr (bottom), using the grism redshifts. The orange model shows an additional 5% enhancement of centrally concentrated Hβ and [O III] emission. The accuracy of the grism redshifts enables us to resolve absorption features at $z \sim 2$ with high signal-to-noise for the first time.

(A color version of this figure is available in the online journal.)

high-resolution models with the grism response and the object morphology in the H_{F140W} direct image (see Brammer et al. 2012b, for more information on how the two-dimensional model spectra are generated). One-dimensional model spectra are then extracted in the same way as was done for the observed G141 spectra. The red line in Figure 2 is the best-fit convolved model with an age of 1.25 Gyr, fit to all wavelengths.

The bottom panel of Figure 2 shows the residuals when subtracting the best-fit model (red). Here, we see the [O III] doublet (λ4959, 5007 Å) and Hβ in emission. It is somewhat surprising to clearly resolve the [O III] doublet given the morphological broadening in the grism spectra. In Figure 3, we demonstrate the expected resolution for the [O III] emission feature at a fixed line ratio of 3:1 when convolving with the interlaced point-spread function (PSF; red) and the average galaxy H_{F140W} profile (black). The stacked profile is constructed by re-centering, masking neighbors, and normalizing by the total flux of individual galaxies before taking the mean/median. The [O III] doublet is blended together when the emission is a global feature of the galaxy, whereas centrally concentrated emission (within roughly the central pixel) shows two clear peaks. The point source nature of the [O III] emission lines also indicates that the high quality of the grism redshifts, as redshift errors would broaden the observed [O III] lines in the stack. We note that although the relative ratio of the [O III] doublet is mildly sensitive to the assumed best-fit model, this effect is significantly less than the error bars from the stacking analysis themselves. The residuals are consistent with both centrally concentrated [O III] and Hβ emission.

To model the central Hβ and [O III] enhancements, we simultaneously fit a grid of Vazdekis et al. (2010) models convolved with the average galaxy profile with enhancements ranging from 0% to 15% above the continuum flux for Hβ and [O III] emission lines convolved with the PSF. We assume a fixed line ratio of [O III] λ5007/Hβ = 1, consistent with the residuals in Figure 2 and line ratio diagnostics for post-starburst galaxies in the SDSS (Mendel et al. 2013). The best-fit model of 1.25 Gyr with a 5% [O III] and Hβ central enhancement is shown in the top panel of Figure 2 (orange).

We measure the [O III] λ5007 line flux from the residuals in Figure 2 to be $1.4 \pm 0.2 \times 10^{-18}$ erg s^{-1} cm^{-2}, which corresponds to $L_{O\,III}$ of $1.7 \pm 0.3 \times 10^{40}$ erg s^{-1} for the median redshift of 1.64. Similarly, we measure the Hβ line flux to be $1.5 \pm 0.2 \times 10^{-18}$ erg s^{-1} cm^{-2}. To determine the line flux errors, we add the simulation errors in quadrature to the error in the average continuum level. The resulting [O III] λ5007/Hβ ratio is 0.9 ± 0.2. If we further correct $L_{O\,III}$ for the average dust extinction value of $A_V = 0.5$ determined from the photometry, we estimate the dust-corrected [O III] luminosity to be $L^c_{O\,III} = 2.4 \times 10^{40}$ erg s^{-1}, following Bassani et al. (1999). Adopting the conversion from $L^c_{O\,III}$ to L_X from Lamastra et al. (2009) and a factor of 10 conversion from L_X to L_{bol} (Lusso et al. 2010), we estimate a typical active galactic nucleus (AGN) luminosity to be $L_{bol} = 2 \times 10^{42}$ erg s^{-1}. However, we note that it is not possible to differentiate between centrally concentrated residual star formation or an AGN without further information.

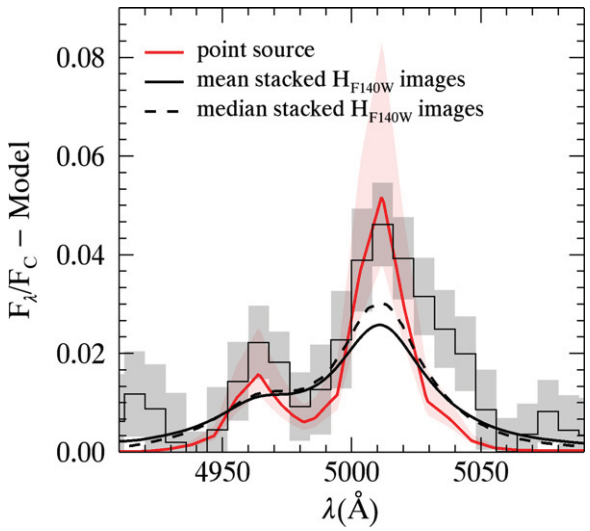

Figure 3. The morphology of the residual [O III] emission after subtracting a 1.25 Gyr model (histogram). The morphology is compared to the expectation for a centrally concentrated gas distribution (red line) and to a distribution that follows the galaxy light (black line). The red shaded region indicates the 1σ confidence interval resulting from the modeling analysis. The resolved double peak of the [O III] feature is only expected for centrally concentrated emission with the low grism resolution.

(A color version of this figure is available in the online journal.)

5. WHAT DRIVES THE SPREAD IN REST-FRAME COLORS?

With these high-quality stacked spectra, we can now begin to assess the driving factor behind the spread in rest-frame colors of quiescent galaxies. The three possibilities include age, dust, or metallicity variations amongst galaxy populations. The difference in rest-frame $U-V$ and $V-J$ colors corresponding to 1 Gyr of passive aging within the Bruzual & Charlot (2003) models results in a 0.4 mag vector parallel to the quiescent sequence. Similarly, increasing the metallicity from $\log(Z) = 0.02$ (solar) to $\log(Z) = 0.05$ or adding 0.5 mag of dust reddening following the Calzetti et al. (2000) dust law results in an almost identical vector in both direction and magnitude. Due to degeneracies between age, dust, and metallicity, it is notoriously difficult to differentiate which of these effects dominates.

Metallicity variations will cause the color spread in galaxies to increase over time as the galaxies passively evolve, reaching a roughly constant scatter for the oldest stellar populations. As noted by Whitaker et al. (2010), the trend for the intrinsic scatter in the rest-frame colors of massive quiescent galaxies to steadily decrease from $z = 2$ to the present epoch (see also, e.g., Ruhland et al. 2009; Papovich et al. 2010) is opposite to that predicted from metallicity variations alone. We therefore expect that metallicity will not have a large effect at high redshifts.

As the shape of the Balmer/4000 Å break depends sensitively on the treatment of dust reddening, one would ideally need to correlate direct, independent measurements of the ages of massive galaxies with their colors. Surprisingly, Bezanson et al. (2013) did not find a simple correlation between the rest-frame color and the strength of the Balmer absorption lines, as some of the reddest galaxies in the spectroscopic sample had strong Balmer absorption lines. However, with a small sample size of 13 galaxies, it is difficult to gauge if these results are representative of the overall quiescent population.

In Figure 4, we plot the median stacked spectra in two rest-frame color bins for the 171 quiescent galaxies, as color-coded in Figure 1. The total number of galaxies in each bin is labeled in Figure 1 and the number of galaxies per wavelength bin is indicated in the top histogram of Figure 4. A minimum number of 20 galaxies was required per wavelength bin to ensure a robust measurement.

Here, we assess the effects of age as a function of rest-frame color for a mass-limited sample of quiescent galaxies by measuring the strength of absorption features such as Mg I and Hβ. Both of these spectral features are sensitive to the age of the stellar population, but not very sensitive to metallicity or dust reddening. Given the narrow baseline of the spectral features, dust extinction is not expected to have a significant effect. At the grism resolution, the Hβ absorption feature is expected to be about 4%–5% stronger in a 1 Gyr stellar population as compared to a 2 Gyr stellar population, whereas the Mg I absorption feature is about 3%–4% weaker. Increasing the metallicity results in a slightly deeper Mg I feature, but only on the order of $\lesssim$1%. To first order, any change measured in Hβ and Mg I is due to age differences between the galaxies.

The average age of galaxies with the bluest rest-frame colors is $0.9^{+0.2}_{-0.1}$ Gyr, consistent with the expectation that they are in the "post-starburst" phase (Kriek et al. 2010; Whitaker et al. 2010, 2012). These galaxies clearly show significantly stronger Hβ and Hγ absorption than the reddest galaxies. Note the difference in shape of the blended G band and Hγ between these two stacks. The redder galaxies are 0.7 Gyr older on average, with a best-fit age of $1.6^{+0.5}_{-0.4}$ Gyr. For a 0.7 Gyr age difference, the Bruzual & Charlot (2003) models predict $\Delta(U-V) = 0.2$ and $\Delta(V-J) = 0.3$, corresponding to exactly the observed difference in the median rest-frame colors of the two bins.

The older quiescent galaxies show clear signs of either central residual star-formation activity or an AGN, while the enhancement in the younger galaxies is not well constrained despite a well-determined spectroscopic age. We measure the residual [O III] λ5007 and Hβ line fluxes for the younger and older populations, finding ratios of 0.3 ± 0.1 and 1.1 ± 0.2, respectively. The bluer galaxies lack a clear [O III] feature, although the difference with the redder galaxies is only marginally significant.

6. DISCUSSION

We present stacked grism spectroscopy of a mass-limited sample of 171 quiescent galaxies at $1.4 < z < 2.2$ from the 3D-HST treasury program (Brammer et al. 2012a). We demonstrate that we can resolve absorption features such as the G band (λ4304 Å), Hβ(λ4861 Å), Mg I (λ5175 Å), and Na I (λ5894 Å) in the median stacks due to the high-quality grism redshifts. We further detect centrally concentrated Hβ and [O III] in emission, indicating either residual central star formation (e.g., Bezanson et al. 2013) or an AGN.

The average $L_{[\mathrm{O\,III}]}$ derived from the stacks of $0.4 \times 10^7\ L_\odot$ is consistent with the results of Mendel et al. (2013), who find that 70%–80% of recently quenched galaxies in the SDSS have LINER-like active nuclei ($L_{[\mathrm{O\,III}]} \lesssim 10^7\ L_\odot$). Furthermore, the [O III] λ5007/Hβ ratio of 0.9 for a median mass of $10^{10.83}\ M_\odot$ places the average quiescent galaxy within the LINER region of the mass–excitation diagnostic diagram (Juneau et al. 2011), albeit marginally consistent with the "composite" crossover region within the error bars. From the average dust-corrected [O III] (λ5007 Å) luminosity, we infer that quiescent galaxies may have a typical AGN luminosity of $L_{\mathrm{bol}} = 2 \times 10^{42}$ erg s^{-1}. These results are consistent with the recent work of Olsen et al. (2013), who find that 70%–100% of massive quiescent galaxies at $1.5 < z < 2.5$ contain a low- or high-luminosity

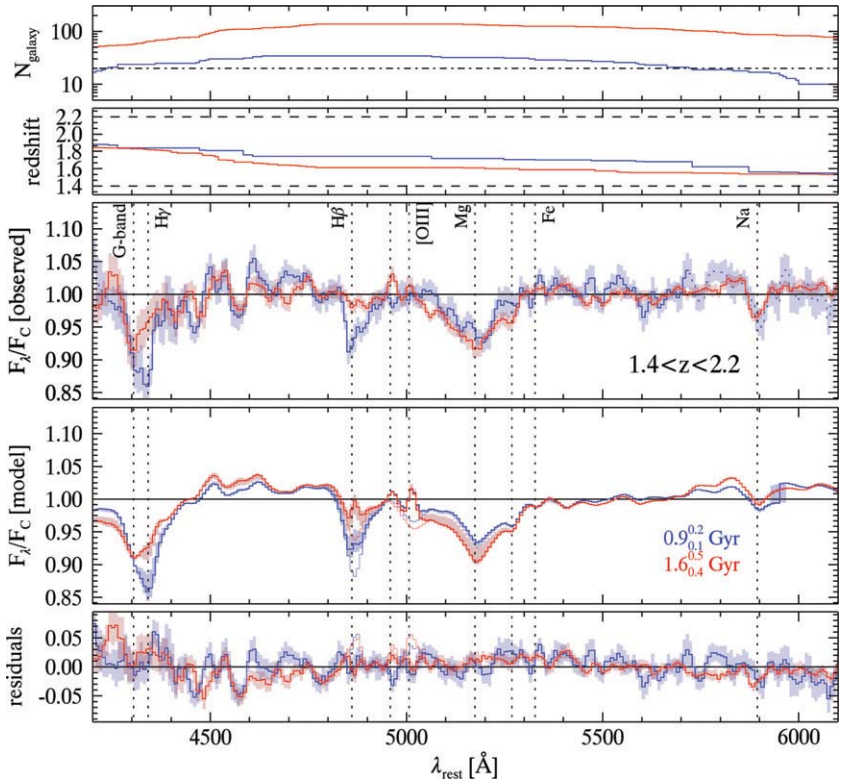

Figure 4. Median stacks of quiescent galaxies in two rest-frame color bins (as defined in Figure 1). The top two panels show the number of galaxies and median redshift of each wavelength bin. The observed stacks in the third panel reveal that the bluest quiescent galaxies have younger ages, most notable by the stronger Hβ and weaker Mg I absorption. The fourth panel shows the best-fit models, including a 5%–6% centrally concentrated enhancement of Hβ and [O III] emission. The residuals are shown in the bottom panel.

(A color version of this figure is available in the online journal.)

AGN. The potential ubiquitous nature of AGNs in massive, quiescent $z \sim 2$ galaxies provides observational support that black hole accretion may be more effective at the high-mass end (e.g., Kriek et al. 2007).

To understand the relationship between rest-frame color and our spectroscopic age measurements, we further stack the data in two rest-frame color bins. We find that the bluest quiescent galaxies have a more prominent Hβ absorption line, with best-fit ages of $0.9^{+0.2}_{-0.1}$ Gyr, confirming the idea that these galaxies are the most recently quenched. Furthermore, we find that redder quiescent galaxies (80% of the population) have an older age of $1.6^{+0.5}_{-0.4}$ Gyr. Although previous spectroscopic studies have measured similarly old ages (e.g., Kriek et al. 2009; Onodera et al. 2012; van de Sande et al. 2012), this is the first time we are able to probe the full population. These results suggest that age varies significantly with the colors of quiescent galaxies, consistent with Whitaker et al. (2010).

Galaxies with the reddest rest-frame colors likely have some degree of dust extinction, as dust-free models cannot produce such red colors at these redshifts. Dust extinction does not greatly affect the line-index measurements for single stellar populations given the narrow baseline of the spectral features, but its effect can be significant for the 4000 Å break (MacArthur 2005). Consequently, although the absorption features of the 3D-HST stacks will be effectively independent of dust extinction, the rest-frame color can change significantly in the presence of dust due to its sensitivity to the continuum shape. We cannot rule out that the reddest galaxies have a potentially significant contribution from younger, dusty quiescent galaxies. Nonetheless, despite this caveat, we measure a significant age difference between the two populations of 0.7 Gyr that is consistent with the observed rest-frame color differences.

The key result from this Letter is that we have conclusively demonstrated that old, quiescent galaxies exist in large numbers at $z \sim 2$. This is not a surprise given extensive previous results that were based on broadband and medium-band photometry (e.g., Brammer et al. 2011), and ground-based spectroscopy for small samples (e.g., Onodera et al. 2012), but our detection of metal lines in the stacked spectrum puts any lingering concerns to rest. Our result also implies that the "UVJ technique," first described in Labbé et al. (2005), is very effective in identifying quiescent galaxies at $z \sim 2$.

We sincerely thank the referee for the thorough review of the manuscript. This research was supported by an appointment to the NASA Postdoctoral Program at the Goddard Space Flight Center, administered by Oak Ridge Associated Universities through a contract with NASA. Support from STScI grant GO-12177 and NASA ADAP grant NNX11AB08G is gratefully acknowledged.

REFERENCES

Bassani, L., Dadina, M., Maiolino, R., et al. 1999, ApJS, 121, 473
Bezanson, R., van Dokkum, P., van de Sande, J., et al. 2013, ApJL, 764, L8
Bower, R. G., Lucey, J. R., & Ellis, R. S. 1992, MNRAS, 254, 601
Brammer, G. B., Sánchez-Janssen, R., Labbé, I., et al. 2012b, ApJL, 758, L17
Brammer, G. B., van Dokkum, P. G., & Coppi, P. 2008, ApJ, 686, 1503
Brammer, G. B., van Dokkum, P. G., Franx, M., et al. 2012a, ApJS, 200, 13
Brammer, G. B., Whitaker, K. E., van Dokkum, P. G., et al. 2011, ApJ, 739, 24
Bruzual, G., & Charlot, S. 2003, MNRAS, 344, 1000
Bundy, K., Scarlata, C., Carollo, C. M., et al. 2010, ApJ, 719, 1969

Calzetti, D., Armus, L., Bohlin, R. C., et al. 2000, ApJ, 533, 682
Cardamone, C. N., Urry, C. M., Schawinski, K., et al. 2010, ApJL, 721, L38
Chabrier, G. 2003, PASP, 115, 763
Cimatti, A., Cassata, P., Pozzetti, L., et al. 2008, A&A, 482, 21
Cimatti, A., Daddi, E., Renzini, A., et al. 2004, Natur, 430, 184
Daddi, E., Renzini, A., Pirzkal, N., et al. 2005, ApJ, 626, 680
Dobos, L., Csabai, I., Yip, C.-W., et al. 2012, MNRAS, 420, 1217
Grogin, N. A., Kocevski, D. D., Faber, S. M., et al. 2011, ApJS, 197, 35
Juneau, S., Dickinson, M., Alexander, D. M., et al. 2011, ApJ, 736, 104
Koekemoer, A. M., Faber, S. M., Ferguson, H. C., et al. 2011, ApJS, 197, 36
Kriek, M., Labbé, I., Conroy, C., et al. 2010, ApJL, 722, L64
Kriek, M., van der Wel, A., van Dokkum, P. G., et al. 2008, ApJ, 682, 896
Kriek, M., van Dokkum, P. G., Franx, M., et al. 2006, ApJL, 649, L71
Kriek, M., van Dokkum, P. G., Franx, M., et al. 2007, ApJ, 669, 776
Kriek, M., van Dokkum, P. G., Labbé, I., et al. 2009, ApJ, 700, 221
Kroupa, P. 2001, MNRAS, 322, 231
Labbé, I., Huang, J., Franx, M., et al. 2005, ApJL, 624, L81
Lamastra, A., Bianchi, S., Matt, G., et al. 2009, A&A, 504, 73
Lusso, E., Comastri, A., Vignali, C., et al. 2010, A&A, 512, A34
MacArthur, L. A. 2005, ApJ, 623, 795
Mendel, J. T., Simard, L., Ellison, S. L., et al. 2013, MNRAS, 429, 2212
Nicol, M.-H., Meisenheimer, K., Wolf, C., et al. 2011, ApJ, 727, 51
Olsen, K. P., Rasmussen, J., Toft, S., et al. 2013, ApJ, 764, 4
Onodera, M., Renzini, A., Carollo, M., et al. 2012, ApJ, 755, 26
Papovich, C., Momcheva, I., Willmer, C. N. A., et al. 2010, ApJ, 716, 1503
Patel, S. G., Holden, B. P., Kelson, D. D., et al. 2012, ApJL, 748, L27
Ruhland, C., Bell, E. F., Häußler, B., et al. 2009, ApJ, 695, 1058
Sánchez-Blázquez, P., Peletier, R. F., Jiménez-Vicente, J., et al. 2006, MNRAS, 371, 703
Toft, S., Gallazzi, A., Zirm, A., et al. 2012, ApJ, 754, 3
van de Sande, J., Kriek, M., Franx, M., et al. 2011, ApJL, 736, L9
van de Sande, J., Kriek, M., Franx, M., et al. 2012, arXiv:1211.3424
van Dokkum, P. G., & Brammer, G. 2010, ApJL, 718, L73
Vazdekis, A., Sánchez-Blázquez, P., Falcón-Barroso, J., et al. 2010, MNRAS, 404, 1639
Whitaker, K. E., Kriek, M., van Dokkum, P. G., et al. 2012, ApJ, 745, 179
Whitaker, K. E., Labbé, I., van Dokkum, P. G., et al. 2011, ApJ, 735, 86
Whitaker, K. E., van Dokkum, P. G., Brammer, G., et al. 2010, ApJ, 719, 1715
Williams, R. J., Quadri, R. F., Franx, M., et al. 2009, ApJ, 691, 1879
Wuyts, S., Labbé, I., Franx, M., et al. 2007, ApJ, 655, 51